Na and Cs intercalation of 2H-$TaSe_2$ studied by photoemission

2001 J. Phys.: Condens. Matter 13 9879

(http://iopscience.iop.org/0953-8984/13/44/305)

INSTITUTE OF PHYSICS PUBLISHING JOURNAL OF PHYSICS: CONDENSED MATTER

J. Phys.: Condens. Matter **13** (2001) 9879–9895 PII: S0953-8984(01)23611-X

Na and Cs intercalation of 2H-$TaSe_2$ studied by photoemission

H E Brauer[1], H I Starnberg[1,5], L J Holleboom[2], H P Hughes[3] and V N Strocov[4]

[1] Department of Physics, Göteborg University and Chalmers University of Technology, SE-412 96 Göteborg, Sweden
[2] Department of Computer Science, Karlstad University, SE-651 88 Karlstad, Sweden
[3] Cavendish Laboratory, University of Cambridge, Madingley Road, Cambridge CB3 0HE, UK
[4] Experimentalphysik II, Universität Augsburg, D-86135 Augsburg, Germany

E-mail: starn@fy.chalmers.se (H I Starnberg)

Received 4 April 2001
Published 19 October 2001
Online at stacks.iop.org/JPhysCM/13/9879

Abstract

The electronic structure of the layered compound 2H-$TaSe_2$ has been studied using angle-resolved photoemission before and after *in situ* intercalation with Na and Cs. Core level spectra verified that Na and Cs both intercalate easily at room temperature, with only small amounts remaining on the surface. Valence band spectra revealed changes in the electronic band structure which were much more extensive than predicted by the rigid band model, but which were in reasonable agreement with theoretical bands calculated by the LAPW method. Some discrepancies between the experimental and calculated results are probably due to intercalation induced changes in the stacking of host layers. A general similarity with results from transition metal dichalcogenides with 1T structure indicates that the intercalation properties are not critically dependent on the internal structure of the host layers.

1. Introduction

One remarkable property of many layered solids is the possibility to intercalate foreign atoms or molecules between the layers. Alkali metal intercalation into the layered transition metal dichalcogenides (TMDCs) is of interest both from a fundamental point of view and for practical applications, e.g. in battery technology, and has been extensively studied for several decades [1, 2]. More recently it has proved possible, by deposition of alkali metals in UHV onto TMDC surfaces, to achieve *in situ* intercalation after an initial adsorption stage [3–5]. The intercalates obtained can be studied with standard surface science techniques. Particularly useful is the possibility to characterize the properties during the reaction from the pure host material to the intercalated compound in a single experimental run.

[5] Author to whom correspondence should be addressed.

In the layered TMDCs, each layer is built up of one sheet of metal atoms with similar chalcogen sheets on both sides, with the transition metal having either octahedral or trigonal prismatic coordination by the chalcogen. $TaSe_2$ belongs to the group V TMDCs, for which both types of coordination occur. The Ta dichalcogenides have received much attention due to the formation of charge density waves (CDWs) [6–8], particularly in the 1T polytypes (octahedral coordination). The 2H polytypes (trigonal prismatic coordination) also exhibit CDWs, but much weaker and at lower temperature. Previous experimental studies of 2H-$TaSe_2$ using photoemission and inverse photoemission have characterized the primarily Se 4p and Ta 5d derived valence and conduction bands, but also shown that the energy and angular resolution must necessarily be high to observe any effect of the CDW [9–16]. This paper presents a detailed photoemission study of 2H-$TaSe_2$ before and after *in situ* intercalation with Na and Cs, where intercalation induced effects on both the valence band structure and the core levels are investigated. As the intercalated alkali atoms enter between the $TaSe_2$ layers, the interlayer separation is significantly increased. Simultaneously electrons are transferred from the intercalants to the host layers. In the rigid band model, the transferred electrons are assumed to enter the lowest available unoccupied levels of the conduction band without significantly changing the host band structure. For VSe_2 and group IV TMDCs, which adopt the 1T structure, experiments and calculations have accumulated a considerable amount of evidence against describing the complicated intercalation process in terms of the rigid band model [17–21], although it may still be useful as a first approximation. An important objective of this study is to investigate whether this applies also to 2H-$TaSe_2$.

2. Band structure calculations

The band structures of pure and intercalated 2H-$TaSe_2$ were calculated using the linear augmented plane wave (LAPW) method within the local density approximation (LDA) of density functional theory. The calculations, which were self-consistent and scalar-relativistic but did not include spin–orbit splitting, used 65 $\boldsymbol{k}$-points in the irreducible part of the Brillouin zone together with 400 LAPW basis functions. The parametrized Ceperley–Alder [22] form of the exchange-correlation potential was used.

The structural parameters used in the calculation for the undistorted phase of 2H-$TaSe_2$ were 3.44 Å (a-axis) and 6.35 Å (c-axis). However, one should note that the unit cell is twice as large perpendicular to the layers, i.e. 12.70 Å.

Regarding the structures of the intercalation compounds, it is known from earlier studies [1] that sites with trigonally prismatic coordination are favoured by Na and K (and most likely also by Cs), but the sliding of host layers which is required to form such sites may be more or less impeded in large single crystals. Without detailed knowledge of the intercalation induced structural changes, we decided to use the simplest possible structure in the calculations: a retained 2H structure with the alkali atoms occupying octahedrally coordinated sites directly in line with the Ta atoms, as illustrated in figure 1. One may argue that changes in the layer stacking and intercalant coordination should be of secondary importance only, compared to the effects of increased layer separation and reduced interlayer interactions [20, 21]. For $NaTaSe_2$ the a and (single-layer) c parameters were set to 3.46 Å and 7.70 Å, respectively, in accordance with experimental values [1]. There are no structural data available for $CsTaSe_2$, but assuming that the in-layer expansion is similar for all alkali metals and invoking some ionic radii considerations for the layer separation, we estimated the a and c parameters to be 3.46 Å and 9.56 Å, respectively.

In figure 2(a) the calculated band structure for undistorted 2H-$TaSe_2$ is presented. Due to the symmetry of the 2H structure, all bands are pair-wise degenerate on the top face of the

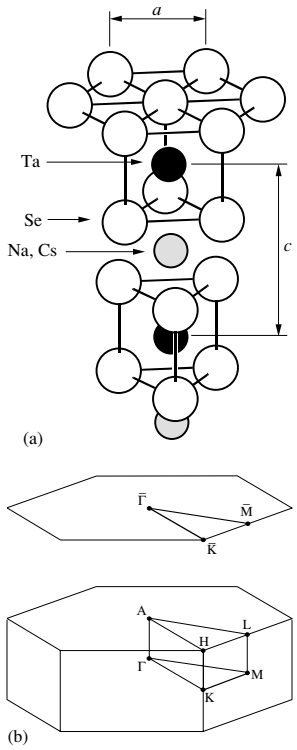

Figure 1. (a) The crystallographic structure of 2H-$TaSe_2$ including the assumed positions of the alkali metal ions after intercalation. (b) The corresponding surface and bulk Brillouin zones.

Brillouin zone (AHL plane) [23]. Two bands (although degenerate in the right half of the figure), labelled Ta $5d_{z^2}$ in the figure, are seen to cross the Fermi level. Immediately below these, with some partial overlap, 12 bands labelled Se 4p are found. An absolute band gap of $\sim$1 eV separates the Ta $5d_{z^2}$ bands from the higher bands labelled Ta 5d.

Our labelling of the bands reflects their predominant orbital compositions, as outlined by Liang [24], but is not strictly accurate, as the band states in general are strongly hybridized with very significant Se 4p components in the Ta 5d bands, and *vice versa*. The labelling of the Ta $5d_{z^2}$ bands is appropriate along the ΓA line, with only minor additional contributions of Se p_z character, but along the KH line these bands are actually dominated by Ta $d_{x^2-y^2}$ and d_{xy} states, as was pointed out already by Mattheiss [25] for the isoelectronic 2H-TaS_2. However, we continue to use the simplified labelling of Liang [24] since it is rather practical, provided that one is aware of its limitations.

The bands show strong in-plane dispersion, but also along the ΓA line (perpendicular to the layers) the calculation yields some bands with significant dispersion. Our band structure resembles the one calculated by Cai and Liu [26], but their bands are generally $\sim$20% narrower. Since the latter calculation used the tight-binding method without self-consistency, this discrepancy is not alarming. Our results are also very close to the band structure for the similar compound 2H-$NbSe_2$, as calculated (self-consistently) by Corcoran *et al* [27]. The most significant difference here is that the uppermost Se 4p band for 2H-$NbSe_2$ reaches slightly above the Fermi level around Γ, while it stays below in our band structure for 2H-$TaSe_2$.

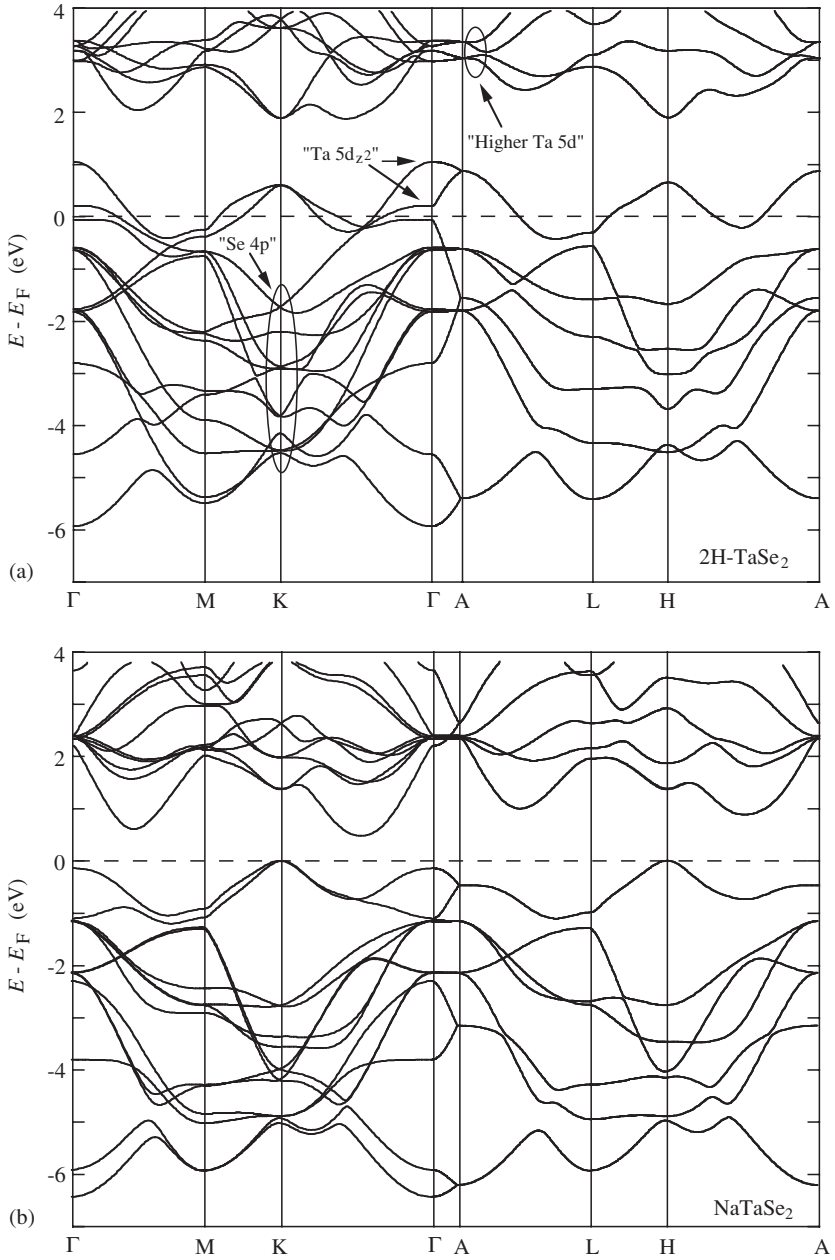

Figure 2. Band structures of (a) 2H-$TaSe_2$, (b) $NaTaSe_2$ and (c) $CsTaSe_2$ calculated with the LAPW method.

Figures 2(b) and (c) show the LAPW band structures for $NaTaSe_2$ and $CsTaSe_2$, respectively. Below E_F they are similar, and apart from the increased filling of the bands, it is notable how the perpendicular band dispersion, e.g. as seen along the ΓA line, is reduced upon intercalation. One remarkable exception from this, however, is that the dispersion of the Ta $5d_{z^2}$ bands along ΓA is unchanged or even slightly increased upon intercalation with Na, probably as a result of hybridization with Na 3s states. The higher conduction bands, above

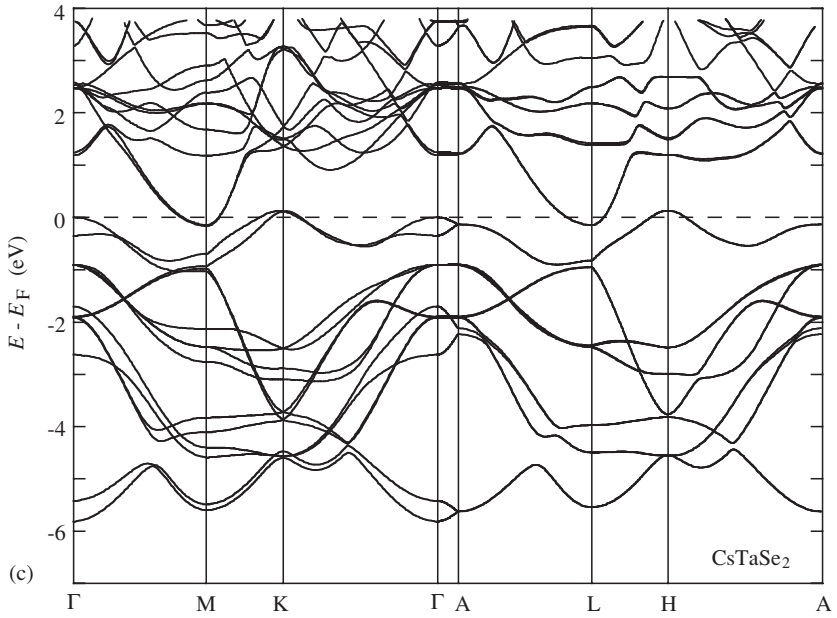

Figure 2. (*Continued*)

E_F, are very different for the two intercalation compounds. These bands are mainly of Ta 5d character for $NaTaSe_2$, but for $CsTaSe_2$ they overlap in energy with the Cs 4f states, and the resulting differences are most likely an effect of hybridization with the latter states. For $CsTaSe_2$ these higher conduction bands have minima (along the ML lines) which are below the maxima of the Ta $5d_{z^2}$ bands (along KH). Consequently, the LAPW calculations predict that the fully intercalated $CsTaSe_2$ is a semimetal, in contrast to $NaTaSe_2$ which should be a semiconductor. It is not clear whether these predictions apply also to structures with altered stacking of the layers.

3. Experimental details

All core level spectra and the valence band spectra from Na_xTaSe_2 were measured at beamline 41 at the MAX synchrotron radiation facility in Lund, Sweden. This beamline includes a toroidal grating monochromator providing photons with energies in the range 15–200 eV. The valence band studies of pure 2H-$TaSe_2$ and Cs_xTaSe_2 were made in a VG ADES 400 spectrometer equipped with a rare-gas discharge lamp. Both spectrometers were typically operated with $\pm 2^\circ$ angular acceptance and $\sim$0.1 eV energy resolution.

Clean mirrorlike surfaces of 2H-$TaSe_2$ were obtained by cleaving single crystals attached to the sample holders by silver filled epoxy in UHV. The crystals were azimuthally oriented by LEED in the $\bar{\Gamma}\bar{M}$ and $\bar{\Gamma}\bar{K}$ azimuths. Na and Cs were deposited *in situ* from carefully outgassed SAES getter sources by resistive heating. In each deposition cycle the Na source was operated at 6.0 A for 2 min and the Cs source at 4.5 A for 3 min. We estimate that in each cycle far more alkali was deposited than required to obtain monolayer coverage. The base pressure in the UHV chambers was typically 1×10^{-10} Torr, but during alkali depositions the pressure increased by a factor of 2–5. The photoemission measurements as well as the alkali depositions were made at room temperature, i.e. well above the transition temperature for the CDW phase. The LEED pattern of 2H-$TaSe_2$ was a sharp 1×1 hexagonal one, which

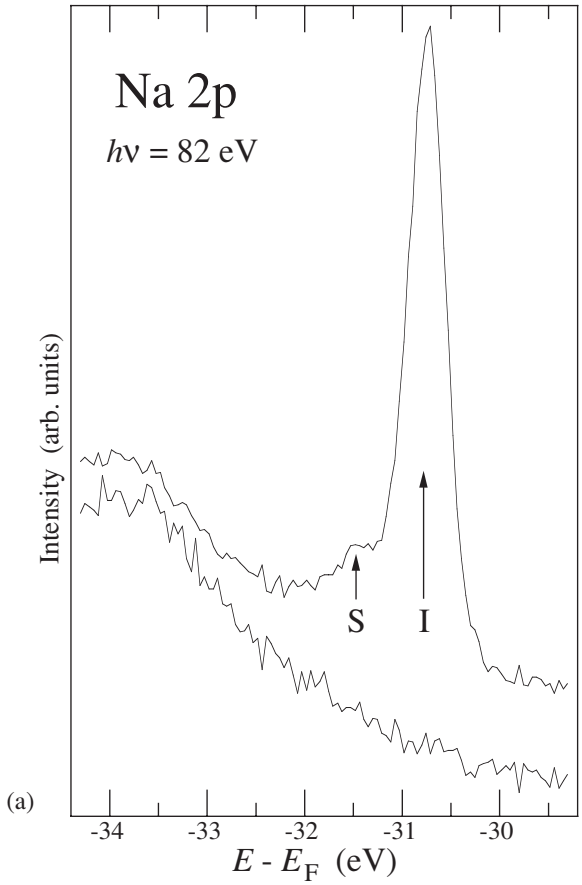

Figure 3. (a) Na 2p core level spectra obtained with $h\nu = 82$ eV after Na deposition onto 2H-$TaSe_2$ (upper curve, the lower shows the background). (b) Ta 4f core level spectra obtained with $h\nu = 82$ eV from (i) pure 2H-$TaSe_2$ and (ii) Na_xTaSe_2. (c) Se 3d core level spectra obtained with $h\nu = 130$ eV from (i) pure 2H-$TaSe_2$ and (ii) Na_xTaSe_2.

confirmed the quality of the cleavage surface. After alkali depositions the LEED pattern was weaker but otherwise unchanged, while the background intensity increased. This indicates that no superlattice was formed, and that the alkali atoms left on the surface were disordered. Due to the absence of dangling bonds the clean surface is very inert, but it appeared that even the alkali-dosed surfaces were remarkably inert, as has been reported previously for other alkali/TMDC systems [19–21, 28]. Several days after the initial alkali depositions, photoemission spectra indicated only moderate contamination.

4. Experimental results

4.1. Core levels

Figure 3 shows core level spectra before and after Na deposition. The deposition was made in two cycles each of 2 min duration at 6.0 A.

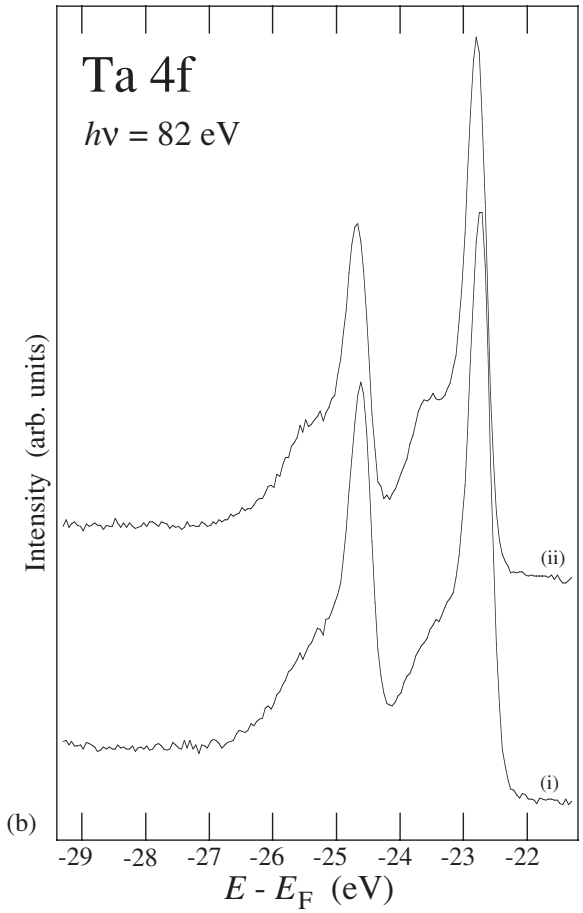

Figure 3. (*Continued*)

The Na 2p spectra in figure 3(a) consists of an intense peak at 30.7 eV binding energy (BE) and a weak shoulder at 31.5 eV.

The Ta 4f spectra before and after the Na deposition are shown in figure 3(b). The deposition changed the lineshape but not the BE of the main peaks. Already for pure 2H-$TaSe_2$ the Ta 4f lineshapes are clearly asymmetric, with apparent shoulders on the high BE side. After the deposition these shoulders became more pronounced, most clearly seen for the $4f_{7/2}$ structure, and shifted to 0.85 eV higher BE relative to the main peaks.

Also the corresponding Se 3d spectra were recorded and are shown in figure 3(c). The Na deposition induced a $\sim$0.25 eV shift towards higher BE, and broadened the lineshape, which was clearly asymmetric both before and after the deposition.

After the Cs depositions we recorded only Cs 5p spectra, as synchrotron radiation was not available during these experiments. These spectra are not shown here, but in agreement with earlier studies [3] they showed two pairs of peaks of which one pair was much weaker and appeared at $\sim$1 eV higher BE than the other pair.

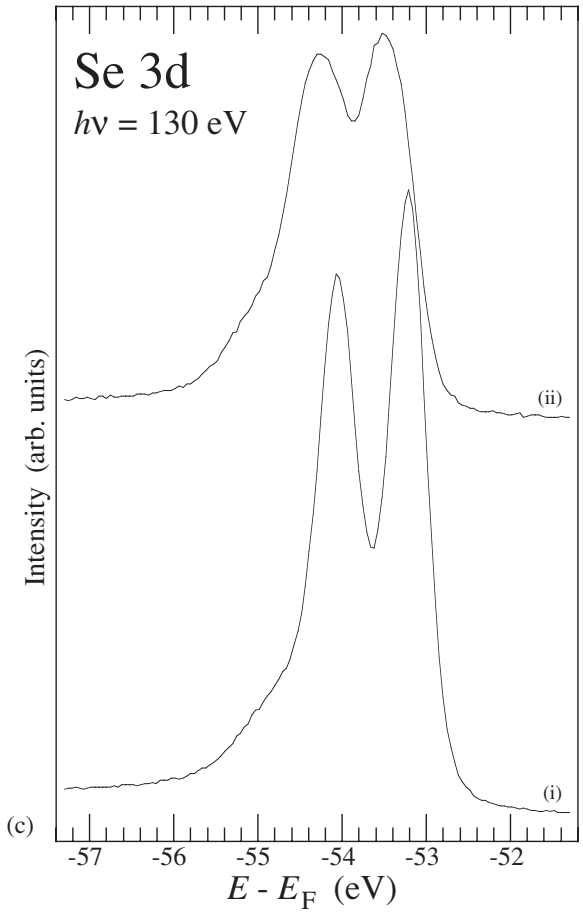

Figure 3. (*Continued*)

4.2. Valence bands

Valence band spectra of pure 2H-$TaSe_2$ were recorded using the He I line ($h\nu = 21.22$ eV) in the $\bar{\Gamma}\bar{M}$ and $\bar{\Gamma}\bar{K}$ azimuths with the emission angle θ in the range -20° to 70°. The intervals between angles were chosen to allow for careful bandmapping. Instead of explicitly showing these spectra, we have summarized them in structure plots, as described in section 5.2.

The valence band spectra after Na deposition were recorded using synchrotron radiation, which enabled measurements of a normal emission series with $h\nu = 20$–40 eV, and are presented in figure 4(a). The Na 2p core level, excited by second-order grating diffraction, overlies some of the spectra and is marked with arrows. Near E_F, emission from the Ta 5d band is seen, in which two spectral features can be distinguished. The emission from the Se 4p bands begins at ∼1 eV BE and several peaks can be observed down to ∼6 eV BE. The observed peaks show no significant dispersion.

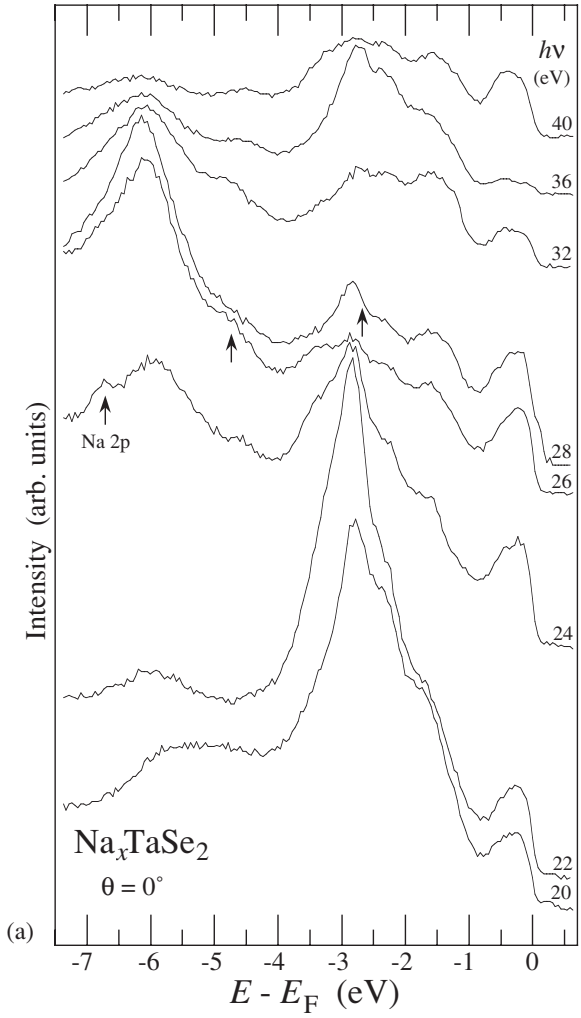

Figure 4. (a) Normal emission valence band spectra of Na_xTaSe_2 recorded with $h\nu = 20$–40 eV. (b) Normal emission valence band spectra of Cs_xTaSe_2 recorded with the Ne I, He I, Ne II and He II lines.

Off-normal emission spectra after Na deposition were measured in the $\bar{\Gamma}\bar{M}$ azimuth, but in analogy with the corresponding series from pure 2H-$TaSe_2$, these results are presented as structure plots in section 5.2.

Normal emission spectra after Cs deposition were recorded using the Ne I, He I, Ne II and He II lines ($h\nu = 16.85, 21.22, 26.8$ and 40.8 eV, respectively). They are shown in figure 4(b), and evidently there is no perpendicular dispersion.

Off-normal emission spectra recorded after Cs deposition were measured using He I radiation ($h\nu = 21.22$ eV) in both the $\bar{\Gamma}\bar{M}$ and $\bar{\Gamma}\bar{K}$ azimuths with the emission angle θ in the range -20° to 70°. As with the other angular series the results are presented as structure plots in section 5.2.

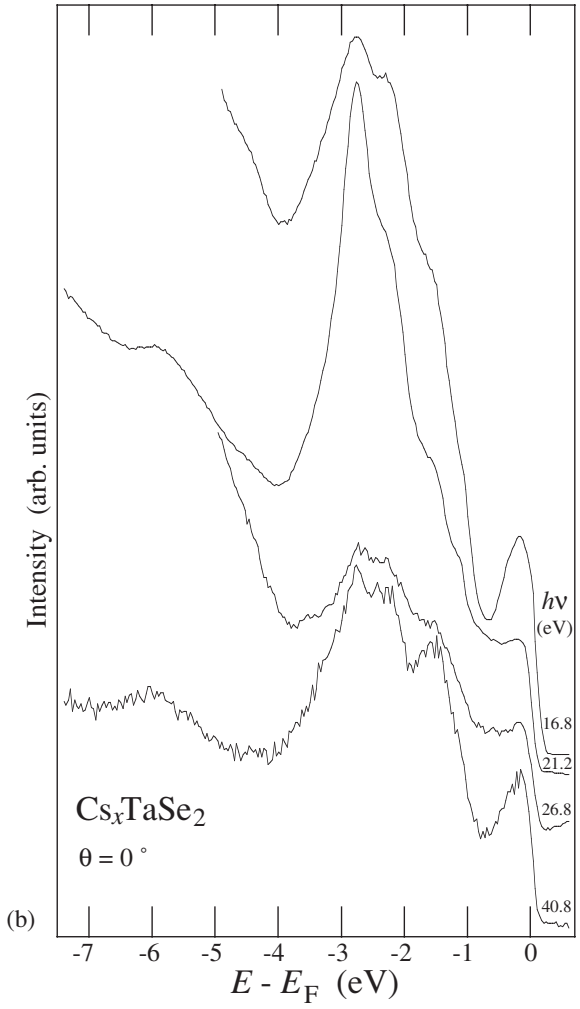

Figure 4. (*Continued*)

5. Discussion

5.1. Core levels

In analogy with other Na/TMDC studies [20, 21, 29] the strong and sharp peak (labelled I) in figure 3(a), with a weaker structure (labelled S) on the high BE side, clearly proves the presence of intercalated Na, but also that only a small amount remains at the surface.

The stoichiometry of Na intercalated 2H-$TaSe_2$ was estimated from the relative spectral intensities of the Na 2p compared to the Ta $4f_{7/2}$ and Se $3d_{5/2}$ levels normalized by theoretical atomic photoionization cross sections [30]. Both comparisons result in the approximate composition $Na_{0.3}TaSe_2$. Similar estimates for Cs intercalated 2H-$TaSe_2$ based on x-ray core level spectra were not successful, and no reliable concentration could be deduced. In [3] the stoichiometry was estimated as $Cs_{0.6}TaSe_2$ based on similar core level intensity comparisons.

However, we believe that the stoichiometry of our Cs intercalated sample was lower and probably similar to what was found for the Na intercalated sample.

Core level lineshapes are modified by the screening of the core hole by the conduction electrons, and this screening depends on the density of states close to E_F. The charge transfer that accompanies the intercalation increases the conduction band filling and obviously alters the density of states near E_F. Due to the different screening properties, it is only natural that the lineshapes of both the Se 3d and the Ta 4f core levels are modified by the intercalation. In addition to the altered screening, the presence of intercalated Na changes the local chemical environment, which also could induce a broadening of the core levels. As the Se atoms are closest to the intercalated Na atoms, this will have larger influence on the Se than the Ta core levels. According to the rigid band model, the density of states at E_F in 2H-$TaSe_2$ should decrease upon intercalation, which should lead to weaker screening and more overall symmetric lineshapes. This is not observed, but instead it must be considered that important modifications of the valence and conduction band structures might be induced. Similar effects have been observed in photoemission studies on alkali metal intercalated VSe_2 [20].

The Ta 4f core level has been studied in detail for the very similar system 2H-TaS_2 and some of its transition metal intercalates [31]. Upon comparison there is a strong resemblance between the lineshapes of Na_xTaSe_2 and $Mn_{1/4}TaS_2$, which could be fitted with one pair of peaks when the detailed configuration of the joint density of states, $J(E)$, was accounted for. It seems therefore plausible that only one pair of peaks is needed to reproduce the Ta 4f lineshape of Na_xTaSe_2 as well.

5.2. Valence bands

The photoemission spectra in the $\bar{\Gamma}\bar{M}$ azimuth agree well with a previous 2H-$TaSe_2$ study with the conduction peak dispersing above E_F near the zone centre [13]. This peak has its highest BE at $\bar{M}$ (around $\theta = 35^\circ$). The valence band spectra show a multitude of structures in both azimuths. The spectral features were converted into structure plots where the initial state energy is plotted versus $k_\parallel$, the wave-vector component parallel to the surface in line with [32]. The experimental structure plots can then be compared to the theoretical LAPW bands. The experimental bands along $\bar{\Gamma}\bar{M}$ are compared to the bands calculated along ΓM (full curves) and AL (dashed curves) in figure 5(a), while the experimental bands along $\bar{\Gamma}\bar{K}\bar{M}$ are compared to the bands calculated along ΓKM (full curves) and AHL (dashed curves) in figure 5(b). As the perpendicular wave-vector component $k_\perp$ is not conserved in the photoemission process, the correct approach is to compare the experimental points to the surface-projected band structure. Due to the absence of band gaps along the hexagonal zone face (AHLA), the surface projected bands are well approximated by the areas between pairs of mid-zone (ΓKMΓ) bands (full curves), which are cross-hatched in figure 5. The bands along the AHLA planes (dashed curves) typically run between the corresponding pairs of (ΓKMΓ) bands, but where exceptions are found the cross-hatched areas are extended out to the corresponding AHLA bands.

A common problem of LDA band-structure calculations for TMDCs is their tendency to underestimate the gap between the chalcogenide p bands and transition metal d bands [21]. To compensate for this, we divided the calculated bands into two groups, the lower one consisting of the Se 4p bands and the higher one consisting of the Ta $5d_{z^2}$ and higher 5d bands. These two groups of bands were then shifted rigidly and independently of each other in order to achieve the best possible agreement with the experimental data. This simple method neglects any hybridization dependent changes in the shape of the bands, but it is justified by the fact that surprisingly good agreement with experimental results is nevertheless found

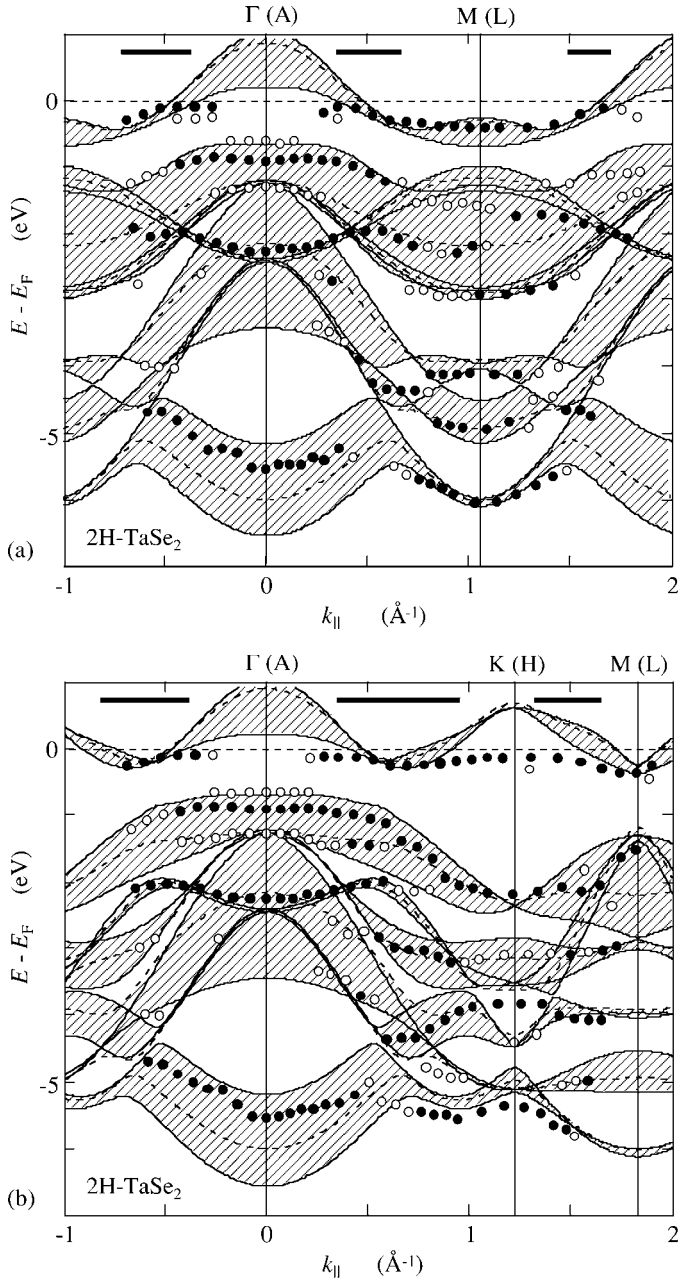

Figure 5. Structure plots of 2H-$TaSe_2$ along (a) $\bar{\Gamma}\bar{M}$ and (b) $\bar{\Gamma}\bar{K}\bar{M}$. Comparison is made with the LAPW bands calculated along (a) ΓM (full curves) and AL (dashed curves) and (b) ΓKM (full curves) and AHL (dashed curves). The surface projected bands are approximated by the cross-hatched areas as described in the text. The horizontal bars at the top indicate Fermi level emission maxima as explained in the text.

in most cases. The good agreement between measured peak dispersions and LAPW bands displayed in figure 5 was obtained by shifting the Se 4p bands down by 0.62 eV, but leaving

the d bands as calculated. The absence of a d band shift is commensurate with the condition that the Ta $5d_{z^2}$ band should be half-filled. All major spectral features can at this stage be clearly identified in terms of their origins.

The Fermi surface of 2H-$TaSe_2$, which is of critical importance in discussions of the CDW transition, has recently been studied by high-resolution photoemission [15, 16]. One problem encountered in this context is that spectral peaks become distorted close to the Fermi level, which makes it difficult to determine with accuracy where in $\boldsymbol{k}$ space the bands cross the Fermi level. An example of this is the existence of a peak immediately below E_F at K(H), as indicated in figure 5(b), despite the fact that the Ta $5d_{z^2}$ band here is expected to be well above E_F. This discrepancy can be attributed to indirect transitions from nearby regions of $\boldsymbol{k}$ space where this band is occupied, but the peak may also result from the band having a tail which reaches below E_F and is reshaped by the Fermi–Dirac distribution function. In either case one may expect the peak to be weaker than if it originated from a band located below E_F, and experimentally we indeed find an intensity minimum close to K(H). Although our measurements were not designed for accurate determination of Fermi level crossings, we could obtain some complementary information by plotting the photoemission intensity at E_F as a function of $k_\parallel$. This intensity should have maxima at the Fermi level crossings, although in practice they tend to be shifted towards the occupied side of the band, due to the limited energy resolution. The positions and widths (full widths at half maximum) of the peaks found in these plots are represented in figures 5(a) and (b) as horizontal bars at the top of each structure plot. The agreement with the calculated Fermi level crossings is reasonable, although the two crossings halfway along ΓK(AH) give rise to one broad intensity maximum rather than two resolved peaks. Better accuracy can in principle be achieved by using more elaborate procedures for data analysis [33, 34], but would require more data and higher resolution to be meaningful.

The dispersion of the valence bands in the direction perpendicular to the layers can be probed by measuring a series of normal emission spectra at different photon energies. In TMDCs there are usually several bands with considerable perpendicular dispersion, which are predicted to decrease upon alkali metal intercalation (see, for example, some of the bands along ΓA in figure 2). In photoemission studies of TiS_2, $ZrSe_2$ and VSe_2, which all have the 1T structure, the effect of alkali metal intercalation has been found to be even more drastic, with almost complete loss of observable perpendicular dispersion [19–21]. The normal emission data for Na_xTaSe_2 and Cs_xTaSe_2 presented in figure 4 show this to be the case for alkali metal intercalated 2H-$TaSe_2$ as well. In analogy with the above-mentioned 1T-polytype TMDCs, the discrepancy with the LAPW results (which predict some remaining perpendicular dispersion) could be due to intercalation induced stacking disorder, which may result from an incomplete transition from the 2H structure to structures with trigonal prismatic coordination of the alkali metal ions. Crystallographic studies have verified that alkali metal (with the exception of Li) intercalation may favour such structure changes in many TMDCs, including $TaSe_2$ [1, 35, 36]. Randomness and inhomogeneities in the layers of intercalated Cs atoms may also contribute to the disorder in the perpendicular direction.

Figures 6 and 7 show the structure plots obtained from the angular series recorded from Na_xTaSe_2 and Cs_xTaSe_2, respectively. Again the calculated Se 4p and Ta 5d bands have been shifted independently in energy to obtain the best possible agreement with the experimental data, and the position and widths of emission maxima at E_F are indicated by horizontal bars as in figure 5. These maxima agree reasonably well with the Fermi level crossings of the LAPW bands.

The fairly good agreement for Na_xTaSe_2 seen in figure 6 was obtained by shifting the LAPW Ta 5d bands up by 0.57 eV and the Se 4p bands down by 0.17 eV. The upward shift of the Ta 5d bands is a consequence of the intercalation being only partial. For the fully

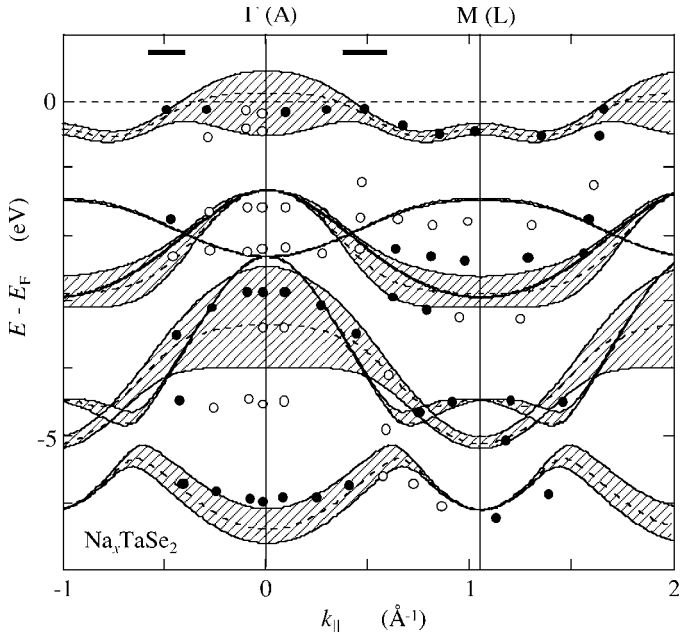

Figure 6. Structure plot of Na_xTaSe_2 along $\bar{\Gamma}\bar{M}$. Comparison is made with the LAPW bands calculated along ΓM (full curves) and AL (dashed curves). Cross-hatched areas and horizontal bars as in figure 5.

intercalated compound $NaTaSe_2$, this band would be completely occupied. The most relevant quantity here is the relative shift of the Se 4p and Ta 5d sets of bands: apparently the LAPW calculation underestimated the gap between them by 0.74 eV. This should be compared to the 0.62 eV discrepancy found for pure 2H-$TaSe_2$. Most experimental peaks can now be identified in terms of their origin. The few remaining points which are not close to any calculated bands are most likely due to indirect transitions from critical points and band edges.

Reasonably good agreement between calculated bands and experimental peak positions were found also for Cs_xTaSe_2, as seen in figure 7. Here the LAPW Ta 5d bands were shifted up by 0.21 eV and the Se 4p bands down by 0.48 eV, meaning that the calculated p–d gap was 0.69 eV smaller than found experimentally. All major features can be identified in terms of their origins, but some significant deviations are clearly seen. The lowest band shows less dispersion than predicted, but the spectral peak is broad and has an angle-dependent asymmetric shape, which makes accurate determination of its dispersion difficult. The deviations seen around K(H), where the peak consistently is found ∼0.6 eV below the calculated band, are large enough to indicate a real discrepancy, however. There are several weak structures appearing in the gaps between calculated bands. Of these, the ones appearing ∼4.5 eV below E_F near Γ(A) and ∼1.7 eV below E_F at K(H) are most likely due to indirect transitions from critical points and band edges. The weak structure seen ∼1 eV below E_F around Γ(A) in both azimuths is possibly due to emission from unintercalated parts of the sample. A different kind of discrepancy is very clearly visible approximately 2 eV below E_F about halfway between Γ(A) and M(L) in figure 7(a). According to the LAPW calculations, two bands with negligible perpendicular dispersion should cross here without any hybridization. Experimentally, two conspicuous peaks are observed, but instead of a crossing there seems to be a hybridization gap of ∼0.4 eV. This implies that the unit cell has a different symmetry than assumed in

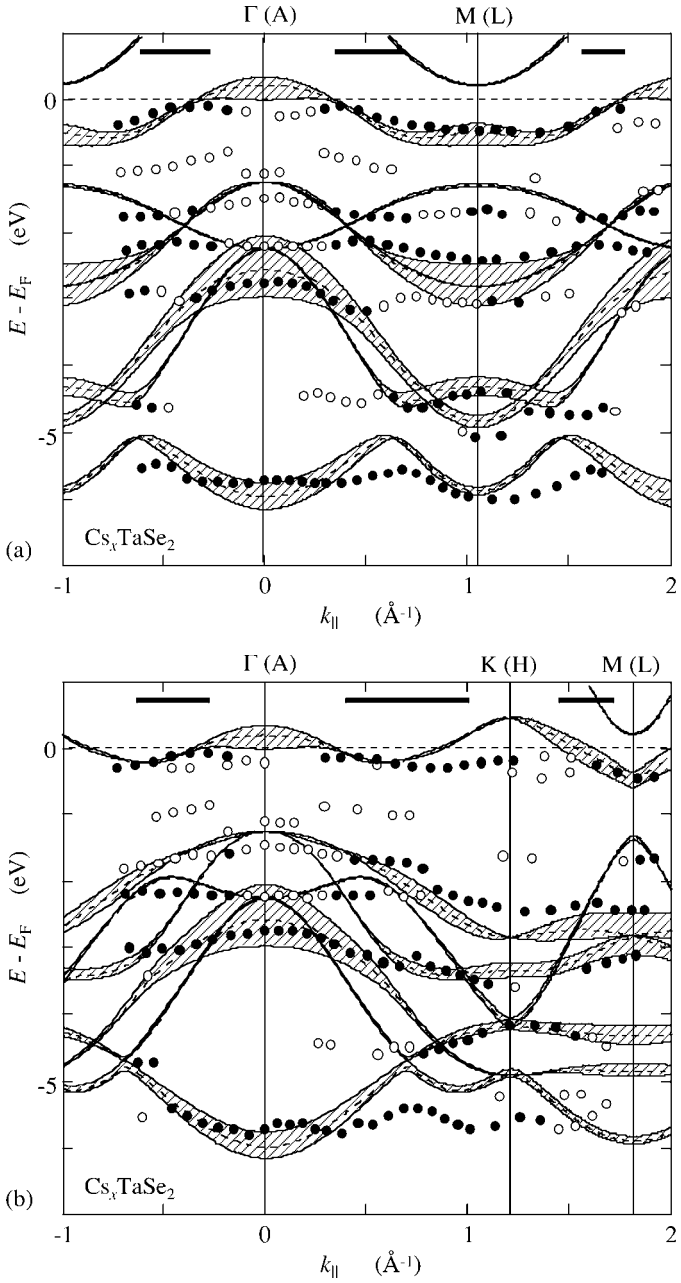

Figure 7. Structure plots of Cs_xTaSe_2 along (a) $\bar{\Gamma}\bar{M}$ and (b) $\bar{\Gamma}\bar{K}\bar{M}$. Comparison is made with the LAPW bands calculated along (a) ΓM (full curves) and AL (dashed curves) and (b) ΓKM (full curves) and AHL (dashed curves). Cross-hatched areas and horizontal bars as in figure 5.

the calculations, and this fits in well with the suspicion that the layer stacking is altered in the intercalation process. LAPW calculations for alternative structures may therefore help to clarify this issue.

It is clear from figures 5–7 that the occupied width of the Ta $5d_{z^2}$ band is increased upon intercalation. The principal reason for this is that the alkali metal valence electrons are donated into the host bands, as anticipated by the rigid band model. But contrary to the assumptions of the rigid band model, it is obvious from the results (in terms of perpendicular dispersion, hybridization, bandwidths and energy gaps) that the host bands are also strongly modified by the intercalation. These significant deviations from the rigid band model are analogous to the changes observed in group IV TMDCs [5, 19–21]. It is furthermore evident from figures 6 and 7 that a significant fraction of the Ta $5d_{z^2}$ band also remains unoccupied after the alkali metal depositions. Complete occupation of this band would require stoichometric intercalation ($x = 1$, as assumed in the calculations), rather than $x \approx 0.3$ as estimated in section 5.1. Considering this difference in band occupation, the satisfactory agreement (with the exception of the Ta $5d_{z^2}$ band filling) between experiments and calculations is quite remarkable. The intercalation induced changes may therefore be described as a major modification of the bands (going far beyond the rigid band model, and probably associated with increased host layer separation and restacking), occurring at a very early stage of the intercalation, followed by gradual filling of the modified bands as more alkali metal is added. The second step in this picture may be viewed as in accordance with a modified rigid band model.

6. Conclusions

Photoelectron spectroscopy has been used to study the electronic structure of the layered compound 2H-$TaSe_2$ before and after *in situ* intercalation with the alkali metals Na and Cs. Both Na and Cs were found to intercalate easily at room temperature with only a small amount of alkali metal remaining on the surface.

The experimental results compared favourably with self-consistent LAPW band structure calculations, although the gap between the Se 4p and the Ta 5d bands had to be manually adjusted (increased by 0.62–0.74 eV) to obtain the best possible agreement. The intercalation resulted in large changes of the electronic band structure, most notably reduced perpendicular dispersion and major changes to bandwidths, band gaps and altered hybridization. Although these changes, which seem to occur at a very early stage of the intercalation, are not at all compatible with the rigid band model, it seems that continued intercalation, once these major changes have taken place, mainly results in increased band filling and thus may be described by a modified rigid band model. The initial large changes to the band structure seem to be associated mainly with the increased layer separation necessary to accommodate the alkali ions, but indications of altered layer stacking were also seen in the experimental results.

In contrast to pure 2H-$TaSe_2$, no significant perpendicular band dispersion was observed in the normal emission spectra after alkali metal intercalation. Apart from the reduced dispersion predicted by the LAPW calculations, this could be an effect of stacking disorder in the intercalation compounds.

Although 2H-$TaSe_2$ has a more complicated structure than VSe_2 and the group IV TMDCs with 1T structure, it seems that the main effects of alkali metal intercalation are completely analogous. This analogy suggests that most of the existing knowledge about alkali metal intercalation of VSe_2 and group IV TMDCs should be applicable to the 2H polytypes of group V TMDCs in general, although systematic studies would be needed to establish this strictly.

Acknowledgments

L Ilver and J Kanski are acknowledged for stimulating discussions. We want to thank F Lévy for providing the 2H-$TaSe_2$ samples and the staff at MAX-lab for their assistance. This work was supported by the Swedish Natural Science Research Council.

References

[1] Rouxel J 1979 *Intercalated Layered Materials* ed F A Lévy (Dordrecht: Reidel) p 201
[2] Friend R H and Yoffe A D 1987 *Adv. Phys.* **36** 1
[3] Pettenkofer C, Jaegermann W, Schellenberger A, Holub-Krappe E, Papageorgopoulos C A, Kamaratos M and Papageorgopoulos A 1992 *Solid State Commun.* **84** 921
[4] Starnberg H I, Brauer H E, Holleboom L J and Hughes H P 1993 *Phys. Rev. Lett.* **70** 3111
[5] Starnberg H I, Brauer H E and Hughes H P 2000 *Electron Spectroscopies Applied to Low-Dimensional Materials* ed H P Hughes and H I Starnberg (Dordrecht: Reidel) p 41
[6] Wilson J A, DiSalvo F J and Mahajan S 1975 *Adv. Phys.* **24** 117
[7] Withers R L and Wilson J A 1986 *J. Phys.: Condens. Matter* **19** 4809
[8] Giambattista B, Slough C G, McNairy W W and Coleman R V 1990 *Phys. Rev.* B **41** 10 082
[9] Smith N V and Traum M M 1975 *Phys. Rev.* B **11** 2087
[10] Hughes H P and Pollak R A 1976 *Phil. Mag.* **34** 1025
[11] Smith N V, Kevan S D and DiSalvo F J 1985 *J. Phys. C* **18** 3175
[12] Nohara S, Namatame H, Matsubara H, Fujisawa M, Naitou M, Tanaka S, Negishi H, Inoue M, Sakamoto H, Misu A and Suga S 1991 *J. Phys. Soc. Japan* **60** 3882
[13] Jakovidis G, Riley J D and Leckey R C G 1992 *J. Electron Spectrosc. Relat. Phenom.* **61** 19
[14] Dardel B, Grioni M, Malterre D, Weibel P, Baer Y and Lévy F 1993 *J. Phys.: Condens. Matter* **5** 6111
[15] Liu R, Olson C G, Tonjes W C and Frindt R F 1998 *Phys. Rev. Lett.* **80** 5762
[16] Liu R, Tonjes W C, Greanya V A, Olson C G and Frindt R F 2000 *Phys. Rev.* B **61** 5212
[17] Umrigar C, Ellis D E, Wang D, Krakauer H and Posternak M 1982 *Phys. Rev.* B **26** 4935
[18] Dijkstra J, van Bruggen C F and Haas C 1989 *J. Phys.: Condens. Matter* **1** 4297
[19] Brauer H E, Starnberg H I, Holleboom L J and Hughes H P 1995 *J. Phys.: Condens. Matter* **7** 7741
[20] Brauer H E, Starnberg H I, Holleboom L J, Strocov V N and Hughes H P 1998 *Phys. Rev.* B **58** 10 031
[21] Brauer H E, Starnberg H I, Holleboom L J, Strocov V N and Hughes H P 1999 *J. Phys.: Condens. Matter* **11** 8957
[22] Ceperley D M and Alder B J 1980 *Phys. Rev. Lett.* **45** 566
[23] Wexler G and Woolley A M 1976 *J. Phys. C* **9** 1185
[24] Liang W Y 1986 *Intercalation in Layered Materials* ed M S Dresselhaus (New York: Plenum) p 31
[25] Mattheiss L F 1973 *Phys. Rev.* B **8** 3719
[26] Cai S-H and Liu C-W 1996 *J. Mol. Struct. (Theochem.)* **362** 379
[27] Corcoran R, Meeson P, Onuki Y, Probst P-A, Springford M, Takita K, Harima H, Guo G Y and Gyorffy B L 1994 *J. Phys.: Condens. Matter* **6** 4479
[28] Brauer H E, Starnberg H I, Holleboom L J and Hughes H P 1995 *Surf. Sci.* **331–333** 419
[29] Starnberg H I, Brauer H E and Hughes H P 1997 *Surf. Sci.* **377–379** 828
[30] Yeh J and Lindau I 1985 *At. Data Nucl. Data Tables* **32** 1
[31] Hughes H P and Scarfe J A 1996 *J. Phys.: Condens. Matter* **8** 1439
[32] Hughes H P and Liang W Y 1973 *J. Phys.: Condens. Matter* **6** 1684
[33] Straub Th, Claessen R, Steiner P, Hüfner S, Eyert V, Friemelt K and Bucher E 1997 *Phys. Rev.* B **55** 13 473
[34] Kipp L, Rossnagel K, Solterbeck C, Strasser T, Schattke W and Skibowski M 1999 *Phys. Rev. Lett.* **83** 5551
[35] Remškar M, Popović A and Starnberg H I 1999 *Surf. Sci.* **430** 199
[36] Pronin I I, Gomoyunova M V, Faradzhev N S, Valdaitsev D A and Starnberg H I 2000 *Surf. Sci.* **461** 137